



**HAL**  
open science

## **Influence of Platinum Group Metals particles aggregation on a glass melt rheological behavior**

Norma-Maria Pereira Machado, Luiz Pereira, Muriel Neyret, Cécile Lemaitre,  
Philippe Marchal

► **To cite this version:**

Norma-Maria Pereira Machado, Luiz Pereira, Muriel Neyret, Cécile Lemaitre, Philippe Marchal. Influence of Platinum Group Metals particles aggregation on a glass melt rheological behavior. *Journal of Nuclear Materials*, 2022, 563, pp.153618. 10.1016/j.jnucmat.2022.153618 . cea-03616919v1

**HAL Id: cea-03616919**

**<https://cea.hal.science/cea-03616919v1>**

Submitted on 23 Mar 2022 (v1), last revised 31 Mar 2022 (v2)

**HAL** is a multi-disciplinary open access archive for the deposit and dissemination of scientific research documents, whether they are published or not. The documents may come from teaching and research institutions in France or abroad, or from public or private research centers.

L'archive ouverte pluridisciplinaire **HAL**, est destinée au dépôt et à la diffusion de documents scientifiques de niveau recherche, publiés ou non, émanant des établissements d'enseignement et de recherche français ou étrangers, des laboratoires publics ou privés.

# **Influence of Platinum Group Metals particles aggregation on a glass melt rheological behavior**

Norma Maria PEREIRA MACHADO<sup>1,2\*</sup>; Luiz PEREIRA<sup>3</sup> ; Muriel

NEYRET<sup>1</sup>; Cécile LEMAÎTRE<sup>2</sup> and Philippe MARCHAL<sup>2</sup>

*1 CEA, DES, ISEC, DE2D, Univ Montpellier, Marcoule, France*

*2. LRGP, UMR 7274, CNRS-Université de Lorraine, Nancy, France*

*3. Department of Earth and Environmental Sciences, Ludwig-Maximilians-Universität*

*München, Munich, Germany*

## **Abstract**

Borosilicate glasses are generally used as matrix to immobilize nuclear fission products resulting from spent fuel reprocessing. In the high-temperature vitrification process (1200 °C), most elements to be confined react chemically with the vitrification additives to form a homogeneous glass melt. Some elements however, such as the Platinum Group Metals particles (PGM: RuO<sub>2</sub>, Pd, Rh), are not incorporated chemically in the molten glass and are present as suspended needle-like or spherical particles of a few microns in the glass melt. The presence of these suspended particles has an impact on the rheological properties of the system leading to a non-Newtonian behavior, which influences the vitrification process. Their impact on the process is the object of characterization and modeling studies.

Studies have established that these suspensions present a shear-thinning and thixotropic behavior. At high shear rate, they behave as suspensions of individual particles, which rheological behavior is controlled by the viscosity of the matrix. On the other hand, at low shear rate, below a stress threshold, and above a certain volume fraction in PGM particles, the formation of aggregates, composed of needle-like Ru/RhO<sub>2</sub> chains and Pd-Rh-Te spherical particles, strongly influences the viscosity of the system.

In the present work, the aggregation mechanisms of a simulated nuclear glass melt containing 3.0 wt% (1.02 vol%) of PGM particles are investigated. The impact of the shear stress and time on PGM aggregation degree is determined using an imposed-stress rheometer at high temperature and imaging analyses via Scanning Electron Microscopy (SEM). Given the difficulties of in situ analysis at 1200 °C, a post-mortem approach is adopted, in which each sample is first submitted to a different shear stress for a certain time interval and then quenched, so that the PGM particles rearrangement can be investigated. For the first time, the interplay between the rheological behavior of the system and the aggregation degree is provided. Based on the acquired experimental data, a force balance computation is executed to illustrate the different aggregation scenarios. This work provides an important input for the modeling and controlling of the vitrification process.

**Keywords:** Melt, Suspension, Platinum Group Metals (PGM), Aggregation, Rheology.

## **1 Introduction**

The vitrification of high-level radioactive waste is the standard immobilization treatment used in France. After the extraction of uranium and plutonium from the spent fuel, the remaining waste is conditioned in a glass matrix in a two steps process. First, the nitrates salts of the waste are converted to oxides at high temperature yielding the calcinate, which is then fed into the melter along with a glass frit leading to the production of a complex amorphous material, that contains around 40 different elements. The melter crucible can be heated by direct induction (hot crucible), indirect induction (cold crucible) or in the Liquid Fed Ceramic Melter with electrodes. The nuclear glass is then poured into metal containers and then stored in wells before their future storage in deep geological formations [1], [2].

Elements and their oxides from the Platinum Group Metals (PGM) such as palladium, rhodium and ruthenium are insoluble in the nuclear glass melt and in the cast glass [3]. They can be found as alloys of palladium and rhodium with tellurium in a spherical form (1 to 5  $\mu\text{m}$ ) alongside with needle-like ruthenium oxide particles (10 to 20  $\mu\text{m}$ ), as shown in Figure 1. The presence of these suspended particles has an impact on several physical properties of the glass melt such as its viscosity or its electrical conductivity [4]. In addition, even if the PGM particles are in small quantities (3 wt%), their tendency to aggregation and sedimentation can lead to the formation of layers of high volume fraction at the bottom of the crucible which can interfere in the process [5][6].

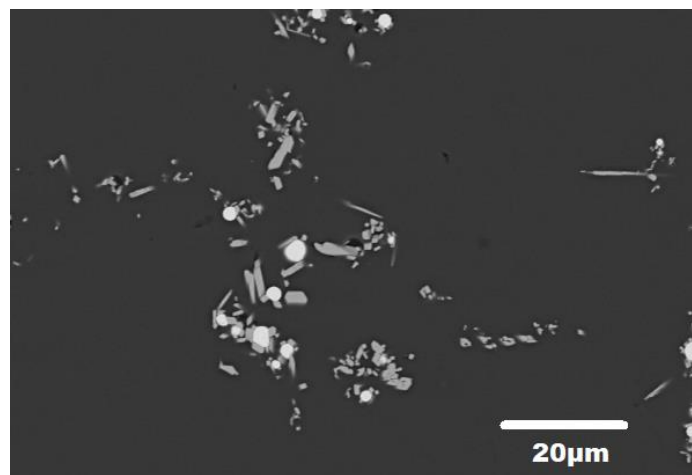


Figure 1 – Scanning Electron Microscopy (SEM) micrographs taken using back-scattered electrons (BSE) mode under 1000X magnification for the technological nuclear glass containing 3 wt% PGM particles after vitrification.

It is therefore essential to understand the impact of the PGM particles on the physical properties of a nuclear glass melt. In particular, the rheological behavior of a fluid can be strongly influenced by the particle aggregation kinetics as well as the flow, which has an impact on the particles collision and clusters destruction. Although the PGM particles lead to significant changes in the rheological behavior of the melt, the literature on the subject is limited due to

the difficulties of high temperature rheological measurements, since most apparatus available are mainly designed to operate with high accuracy at room temperature [7]. Nonetheless, some authors discovered an increase of the system viscosity in the presence of PGM and a non-Newtonian behavior of the material [4], [5], [8]–[10]. Aiming to explore a broader shear rate range needed for the cold crucible melter development, recent studies proposed a new phenomenological model for the rheological behavior of these materials [8], [11].

Puig *et al.* and Hanotin *et al.* studied the viscosity of simulated nuclear glass melts containing PGM particles as a function of the particles content and the temperature [8], [11]. The obtained rheograms showed a shear-thinning behavior and two Newtonian plateaus at low and high shear rates, which were well described by a simplified Cross model with  $n=1$  [12]. At low shear rates and above a certain content of PGM particles, macroscopic aggregates appear, made of  $\text{RuO}_2$  and Pd-Te chains, separated by thin layers of liquid which strongly increase the viscosity of the systems. Temperature in this first case favors aggregation through Brownian motion and consequently, an increase in temperature increases the viscosity of the system. At high shear rates, the system behaves as a suspension of small clusters and individual particles and its viscosity is entirely controlled by the viscosity of the matrix, decreasing for higher temperatures.

Particles aggregation can be induced by external and internal factors, but the aggregation is an inherent behavior of any colloid system, though the extent to which this aggregation prevails may largely differ depending on the particles nature [13]. For the PGM system, authors [8] stated that particle aggregation is a result of an interplay of different forces, such as van der Waals forces and hydrostatic forces. For identical particles, the former is always attractive and the latter, depending on their intensity, may favor or not particle aggregation [14], [15].

Several in situ methods are available to study aggregation phenomena by combining rheometry with different characterizations such as ultrasonic velocimetry, X-ray computed tomography, image analysis, and others [16]–[18]. Nonetheless, these techniques are available at room temperature or below 100 °C, which is much lower than the temperatures of glass melts (900 °C – 1250 °C). In this work, techniques adapted to the high temperatures are employed to characterize particle aggregation in charged glass melts. The impacts of time and shear stress on the PGM particles aggregation are studied for a simulated nuclear glass melt at 1200 °C. A deep analysis of the aggregates and their contribution in the proposed rheological model based on the phenomenology of the system is presented. It consists in estimating the aggregation degree of the PGM particles as a function of time and shear stress. The interplay between the rheological behavior of the system and the aggregation degree is presented for the first time. It provides an important input for the modeling and control of the vitrification process.

## **2 Experimental Method**

### *2.1 Materials*

The material used in this study is a simulated nuclear glass containing 3 wt% of PGM particles. The glass was elaborated on the full-scale pilot unit installed at CEA Marcoule [19]. The process followed the two steps vitrification protocol at 1200 °C using the indirect induction technology. The glass was cooled at room temperature and the studied material was extracted from the middle of the canisters. During the vitrification, the ruthenium presented in the glass as needle-like RuO<sub>2</sub> ranging from 10 to 50 μm, while Pd-Te alloys appeared as spherical particles with diameter ranging from 1 to 10 μm. The theoretical chemical composition of the nuclear glass is shown in Table 1.

Table 1 – Chemical composition of the nuclear glass samples containing 3 wt% of PGM particles.

Glass with 3 wt% PGM									
SiO <sub>2</sub>	B <sub>2</sub> O <sub>3</sub>	Na <sub>2</sub> O	Al <sub>2</sub> O <sub>3</sub>	Alkali metal	Alkaline earth	Rare earth	RuO <sub>2</sub>	Pd	Others
(wt%)	(wt%)	(wt%)	(wt%)	oxides (wt%)	metal oxides	oxides	(wt%)	(wt%)	(wt%)
					(wt%)	(wt%)			
43.7	13.2	9.2	4.2	3.3	5.0	7.0	1.8	1.2	11.4

## 2.2 Rheological measurements

Different aggregation degrees were generated by submitting the samples to several shear stresses during different time intervals at 1200 °C, followed by a fast cooling of the sample to “freeze” the particles rearrangement for further image analyses. The high temperature experimental apparatus used for this work is showed in Figure 2 [11]. It consists of a stress-imposed rheometer (Rheometrics Scientific SR5000) above a tubular furnace that can be heated up to 1500 °C. A tool was designed to ensure the torque transmission from the rheometer to the crucible without disturbances effects. The characterization cell consists of an alumina crucible (diameter, height, and wall thickness equal to 27, 40, and 2 mm respectively) previously filled with glass, centered inside the furnace. The rotor is a multiblade agitator, used in order to maintain a uniform distribution of particles in the glass and avoid settling phenomena [11]. From the top to the bottom of the crucible, the temperature gradient is lower than 2 °C. For these experiments, disposable alumina crucibles are adopted, so that the frozen charged glass and the crucible can be cut at the end of the experiment in order to analyze the PGM distribution in the glass. The rheological parameters such as shear stress ( $\sigma$ ), shear rate ( $\dot{\gamma}$ ), and shear strain ( $\gamma$ ) are linked to measured parameters, namely the torque ( $C$ ) and the angular velocity ( $\Omega$ ) through geometrical factors  $K_\sigma$  and  $K_\dot{\gamma}$ ,

$$\sigma = K_\sigma C \quad \dot{\gamma} = K_\dot{\gamma} \Omega$$

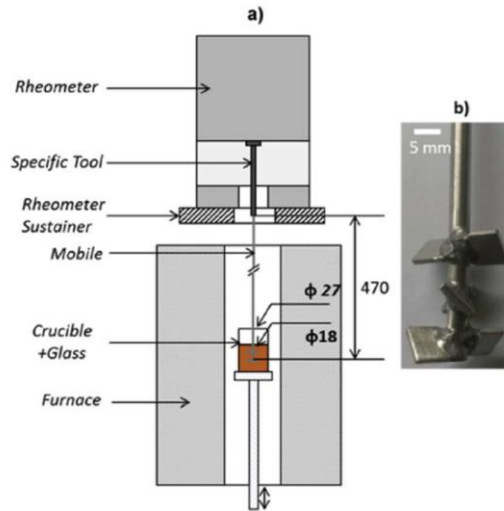


Figure 2- a) High temperature rheological experimental set-up (dimensions in mm), b) Multiblade rotor. [11]

The combination of the crucible and the multiblade geometry forms a virtual Couette cell, therefore factors  $K_{\sigma}$  and  $K_{\dot{\gamma}}$  may be determined through the Couette analogy [20], solving the equation of motion. The boundary conditions are imposed by the geometrical dimensions of a virtual inner cylinder (the rotor) and the outer cylinder (the crucible), in the case of Newtonian fluid or a well-characterized power law fluid [21]. A complete description of the equipment and calibration procedure was provided in Puig *et al* [11].

In order to establish the overall rheological behavior of the material, a first measurement was made in steady state regime by imposing successive shear stress values, from 0.3 to 300 Pa during 600 s, using the Platinum crucible. The temporal evolution of the aggregates was then investigated along with the viscosity. In order to create the different aggregation degrees, the measurements are carried out in transient state regime by imposing to each sample a different shear stress during different time intervals. All samples were first submitted to a pre-shear of 200 Pa during 300 s to disperse completely the PGM particles in the glass melt. Then, the sample was subjected to a given shear stress, between 0.1 to 200 Pa. The experiment duration for each selected stress was chosen considering the thixotropic behavior of the glass melt. For

a given stress level, experiments were repeated 3 to 4 times during different times from 300 s to 7200 s. Table 2 shows the chosen shear stresses and time intervals. Each stress/time pair corresponds to a different experiment and to a new crucible, totaling in the end twenty different experiments.

Table 2 – Operating conditions (shear stress level and duration) for the 20 performed experiments.

<b>Stress (Pa)</b>	<b>Duration (s)</b> (All samples were first pre-sheared at 200Pa for 300s)				
0.1	-	1200	3600	-	7200
2	-	1200	3600	5400	7200
5	300	1200	3600	-	-
10	300	1200	3600	-	-
100	300	1200	3600	-	7200
200	300	1200	3600	-	-

After the shearing period, the rotor is slowly removed from the crucible at a low ascensional velocity of  $8 \text{ mm}\cdot\text{min}^{-1}$  to avoid significant changes in the melt during the withdrawal. The same velocity is used for all the samples, and the cooling of the crucible is performed at the same constant speed for all the samples. The crucible is located on an alumina holder that comes out from the bottom of the furnace. Aiming for a compromise between a quick temperature drop and the preventing of a thermal shock [22], this descent is conducted at a speed of  $2 \text{ cm}\cdot\text{min}^{-1}$ , equivalent to a cooling rate of  $35 \text{ }^\circ\text{C}\cdot\text{min}^{-1}$ . At this rate, no significant changes in the particles rearrangement are expected due to the rapid increase of the glass viscosity at lower temperatures.

### 2.3 Sample preparation

To relieve residual internal stresses introduced during the cooling and avoid breakage during the sample preparation, the glass is submitted to an annealing at 580 °C for 2 h followed by a slow cooling at 10 °C.h<sup>-1</sup> until room temperature is reached. To observe the PGM particles distribution in the crucible, it was filled with epoxy resin and cut with a circular diamond saw in two halves as displayed in Figure 3. One of the halves was cut again horizontally and covered with epoxy resin to fit and to facilitate its support in the SEM measurement cell. The face to analyze was polished and coated with a thin film of carbon for SEM analysis. Each experiment thus produces two samples: the top and the bottom of the crucible (P1 and P2, as shown in Figure 3). The second half of the crucible is kept in case further characterization is needed.

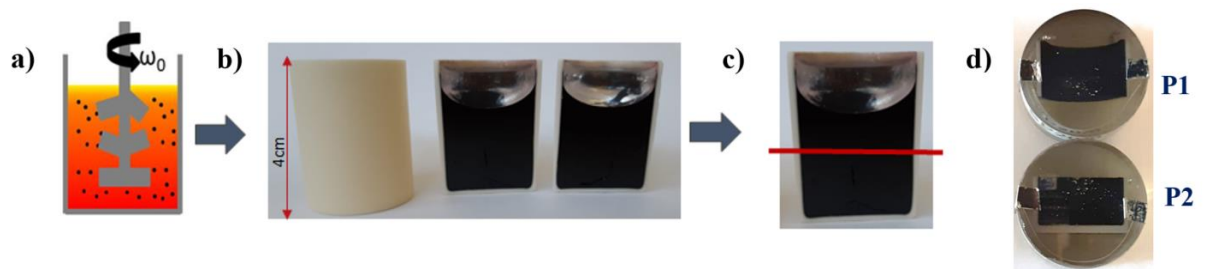


Figure 3 – Samples preparation protocol: the glass melt in the alumina crucible is sheared for a certain time (a). After annealing, the crucible is cut vertically (b), and then cut again horizontally (c), yielding two samples for each crucible (d): top (P1) and bottom (P2).

#### 2.4 Scanning Electron Microscopy (SEM) imaging

The Scanning Electron Microscopy (SEM) was performed using a Zeiss Supra 55 FEG. The image of the whole surface was reconstructed from a mosaic of small images automatically acquired using the commercial SEM software to describe the PGM particles rearrangement in the most representative area. The most representative zone of P1 and P2 was then selected. To ensure a standardization of the procedure, the same rectangular region of each crucible was chosen for all experiments. A final surface of 1.75 cm<sup>2</sup> was selected for the bottom and the top

samples. The union of both surfaces corresponds to the middle of the crucible, *i.e.*, the zone where the rotor was located during the rheological measurement. The analyzed area of the upper sample P1 is located 0.3 cm below the crucible top while the analyzed area of the lower sample P2 lies 0.3 cm above the crucible bottom. Each image that composes the mosaic was acquired at BSE mode under a magnification of  $\times 100$ , an acceleration of 15 kV and a  $1024 \times 768$ -pixel resolution. Each mosaic contained an average of 320 images, with an acquisition time of 10.3 s/image. Due to the size of the sample, a compromise was made between image capturing time and resolution. The Fiji software was used to treat and analyze all mosaics. The methodology of image acquisition and treatment was borrowed from crystallization studies involving image analysis found in the literature [23][24]. Subsequently, the obtained information on the PGM particles were used as input in a Python script, developed to quantify the aggregation degree of the samples for different studied situations.

### **3 Results and Discussion**

#### *3.1 Generation of different aggregation degrees*

From the first steady state viscosity measurements performed on the glass with 3.0 wt% of PGM at 1200 °C (Figure 4), six different conditions are selected, expected to produce six different aggregation degrees. The viscosity curve shows three distinct zone: a Newtonian plateau at low shear rates (marked as M1 in Figure 4), a shear-thinning behavior at intermediate shear rates (M2), and a second Newtonian plateau at higher shear rates (M3). Two shear stresses are chosen in each zone, yielding six different representative stress values, marked with grey stars in Figure 4: 0.1 Pa and 2 Pa in zone M1, 5 Pa and 10 Pa in M2, and 100 Pa, and 200 Pa in M3.

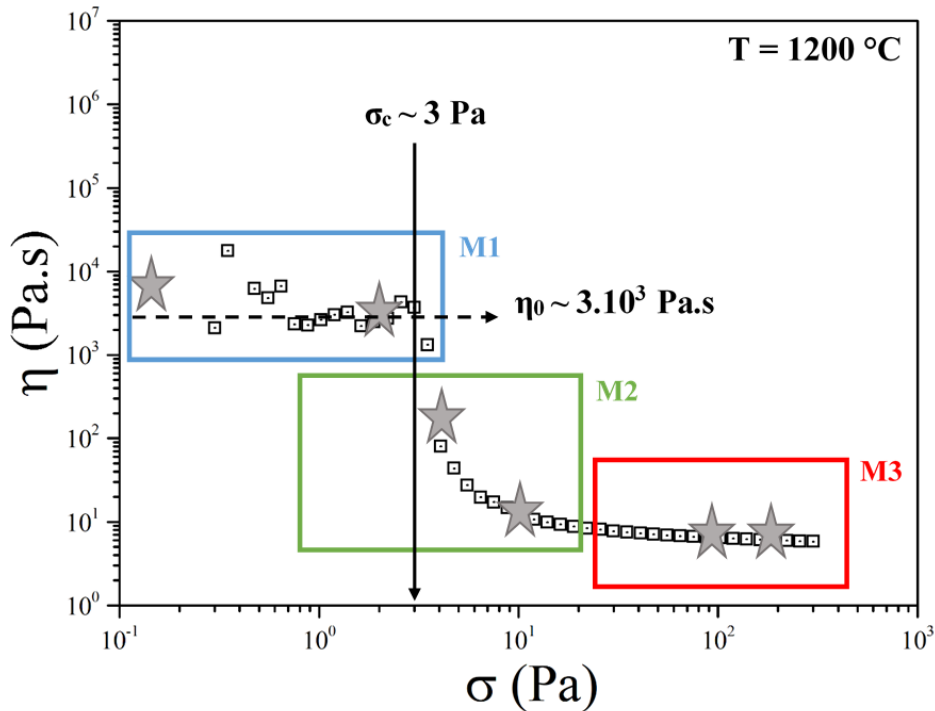


Figure 4 - Evolution of the system viscosity as a function of the shear stress for a 3 wt% of PGM particles at 1200 °C. Stars represent the shear stresses selected for the aggregation analysis.

One of the main obstacles of a non “in situ” measurement is to guarantee the reproducibility of the experiment since for each combination of stress and time, a different sample (in a new crucible) is submitted to the protocol. This is why the tests are repeated at least 3 times, leading to twenty experiments. Figure 5 shows the viscosity of the melt under a shear stress of 5 Pa during three different times: 300, 1200, and 3600 s. It appears that all three curves overlap, which indicates that the three experiments give the same rheological response and the methodology reproducibility is guaranteed. It also shows that three main events were captured by the experiments: the beginning of particles rearrangement, the increase of viscosity and its stabilization. The thixotropic behavior is less pronounced for the higher stresses, but all studied samples showed the same reproducibility.

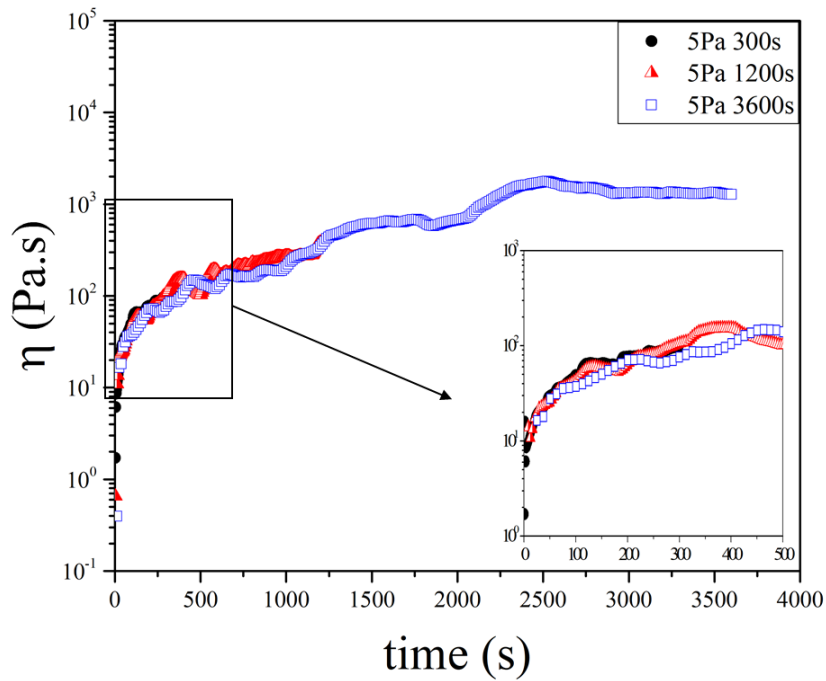


Figure 5 – Evolution of viscosity in time at the imposed stress of 5 Pa for three different samples tested during 300 s, 1200 s and 3600 s. The zoom focuses on the overlap of the three curves, indicating the reproducibility of the experiments.

### 3.2 Determination of the aggregation degrees

All samples were analyzed via scanning electronic microscopy technique. For each experiment, an image was extracted from the bottom and from the top of the crucible, as explained in section 2.4. Although the SEM images give details of the PGM particles in the glass, it is difficult to identify the aggregates only visually. The  $\text{RuO}_2$  needles and the Pd-Te spheres are dispersed in the glass matrix normally in groups, as shown in Figure 6a. They are rarely found separately. It was established that the union of these particles forms a structural unit (SU), which may in turn aggregate with other SUs. Thus, if the goal is to observe the aggregation degree of a sample, an image treatment is necessary to detect the individual SUs, as shown in Figure 6b.

The image treatment consists in detecting the contours of these clusters so that they can be counted and characterized by the software (Figure 6c). In the end, important characteristics of

the sample are obtained such as total area and position of the SUs, using the image analysis tool. Since they do not have a specific format when grouped, the SUs are analyzed as in terms of F eret characteristics (Figure 6d), where their diameter is calculated, as well as the perimeter, mass center, position, and circularity. These properties obtained by the image treatment can be used as an approach for defining the aggregation degree of the samples as will be specified later on.

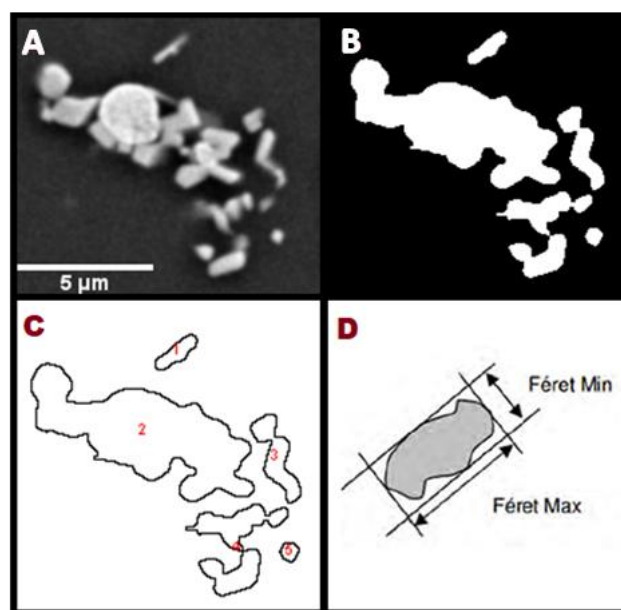


Figure 6 – Example of the image treatment applied to the SEM images to identify the structural units of PGM particles: a) Raw image from SEM. b) The same image after treatment with the Fiji program. c) Contours of the SUs after treatment. d) An example of the F eret form.

Another advantage of the image treatment is the contrast that is created between the particles and the glass matrix by binarizing the mosaic. It produces a resourceful way to analyze by a visual approach the aggregation degree of the samples. Figure 7 shows an example of the obtained mosaics after image treatment for samples subjected to a 5 Pa stress during three different times (300, 1200, and 3600 s). In the images, the PGM particles are shown in white and the glass matrix is black. All samples started from a dispersed state after a strong pre-shear (200 Pa during 300 s). As shown in Figure 7a, after 300 s at 5 Pa, a slight rearrangement of the

particles starts, but the sample is still homogenous comparing the top and the bottom. The particles regroup more significantly after 1200 s, as shown in Figure 7b, where a large glass matrix area (black) is observed, separating the particles in large groups. Besides, the top and the bottom of the crucible is more heterogeneous than the previous situation. For the last sample (5 Pa stress imposed during 3600 s), the sample is completely aggregated and the difference between the top and bottom clearly indicates a sedimentation of the particles (Figure 7c). Although the images were taken from different crucibles, they seem as if they originate from the same crucible but at different times, which helps understanding the impact of time in the rearranging of the PGM. For all studied stresses, mosaics of images were made for each time interval, but the particles evolution was different, highlighting different mechanisms. The aggregation kinetics is strongly influenced by the imposed stress and the forces acting in the melt. For stresses in a close range, these differences may be hard to distinguish using only SEM images. Hence, a numerical tool is necessary to deepen the analysis.

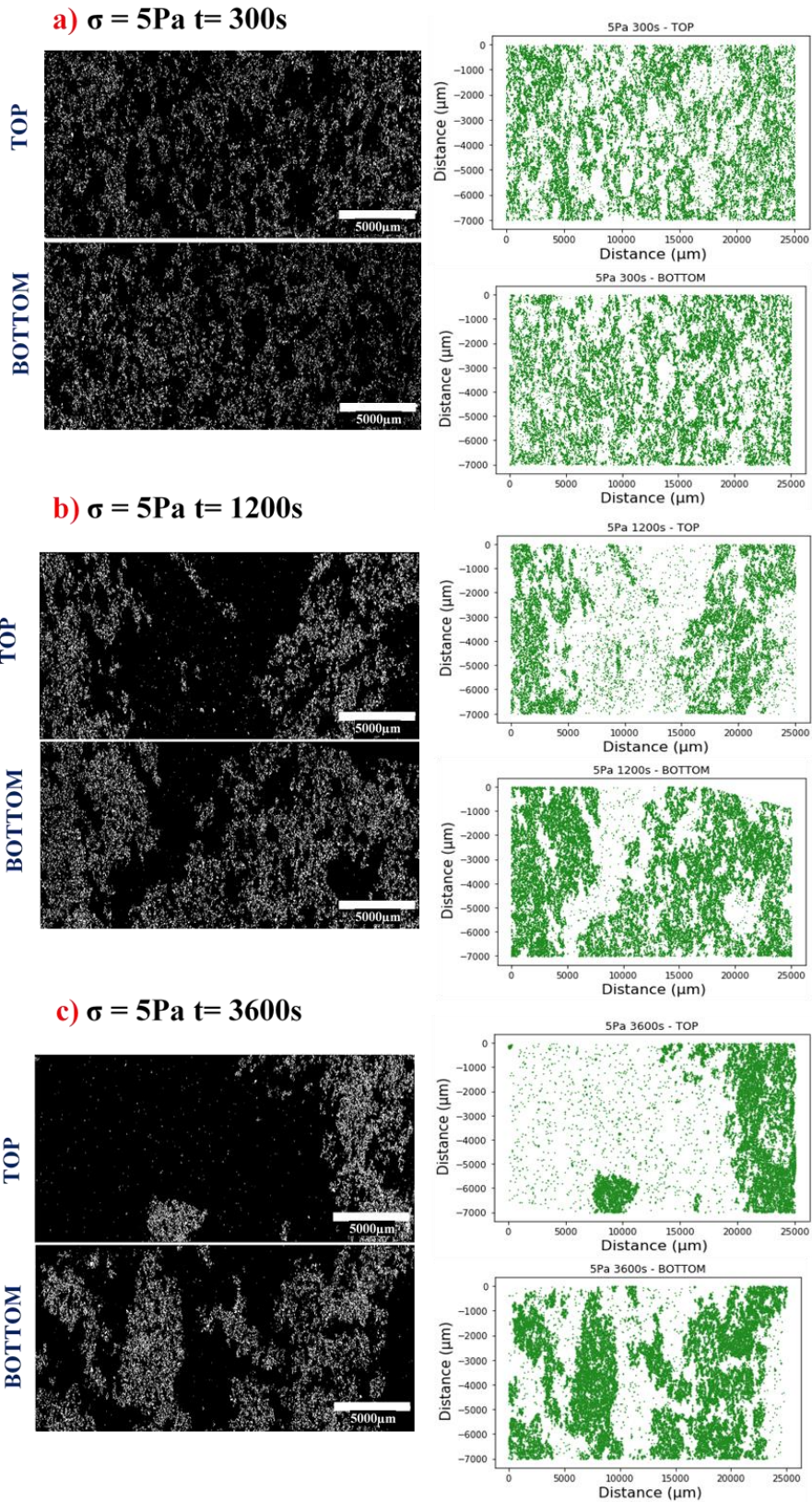


Figure 7 – Top and bottom SEM images (left column) of the sample subject to 5 Pa stress for 3 different durations, binarized via image treatment, along with their corresponding Cartesian representations (right column) of the PGM structural units positioning. Durations of the tests: a) 300 s b) 1200 s, and c) 3600 s.

### *3.3 Impact of time and shear stress in the aggregation degrees*

A Python script was then developed to post-process the treated SEM images, in order to quantify particle aggregation and the macrostructural characteristics of the suspension. This script uses as input the Cartesian coordinates of the SUs in the images and through special geometry calculations, aggregation parameters are obtained, in particular the average distance distribution of the particles to their first neighbor (D1stN), which is a measurement of the distance between the SUs. This distance distribution provides an idea of the level of rearrangement of the particles and an information on the aggregation degree. Indeed, the aggregates are formed by a reunion of smaller clusters that do not necessarily touch one another. The script consists in three steps:

1. Reading of the SUs positions from the image in a Cartesian plane, as shown in Figure 7 for the samples at 5 Pa.
2. Random selection of  $n$  SUs belonging to the population of particles.
3. Calculation of the average distance distribution of the particles first neighbor (D1stN)

The amount of SUs in each image is around 40000 for all experiments. In order to limit the computational effort required to evaluate such a large matrix,  $n = 8000$  random SUs were chosen. The calculation is repeated five times for each image and the standard error associated is calculated. For each stress, two samples are produced from which two D1stN are calculated: one for the top (T) and one for the bottom (B) of the crucible. Figure 8a presents the results for the 5 Pa samples over time. As previously mentioned, when analyzing the 5 Pa images, there is

a difference between the top and the bottom of the crucibles, probably due to sedimentation effects. Nonetheless, the D1stN shows the same evolution in time for both parts of the crucible. If considering the particles aggregation shown in Figure 7 for the same samples, it is coherent that the distance decreases with time since the particles are approaching each other. The longer the crucible is submitted to 5 Pa, the more the particles rearrange to form larger and fewer aggregates. This also illustrates the validation of the average distance distribution of the particles first neighbor as one method to characterize the aggregation degree of the samples.

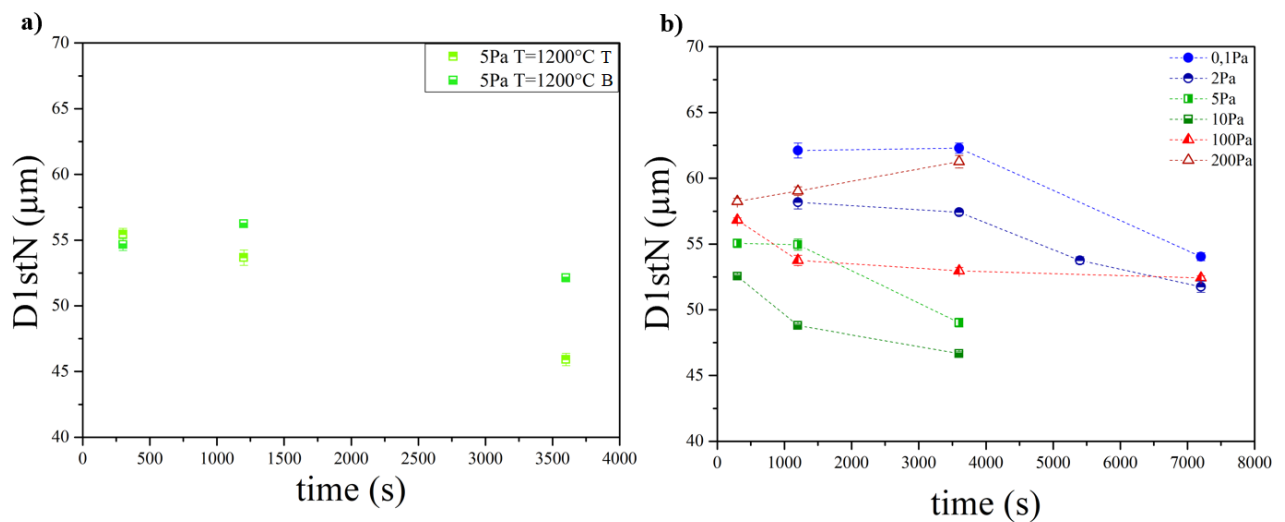


Figure 8- a) Average distance distribution of the particles first neighbor for the 5 Pa samples as a function of time for the top (T) and the bottom (B) of the crucible. b) Average distance distribution of the particles first neighbor for all the studied stresses as a function of time.

For all analyzed samples, both parts of the crucible exhibited the same tendency. The average D1stN was thus calculated for the two crucible parts to indicate the general behavior of the sample and to simplify the data analysis.

In Figure 8b, the D1stN is shown as a function of time for all the experiments. Firstly, a decreasing tendency of the distance with time and with stress is noticed for stresses up to 10 Pa. For an imposed stress of 100 Pa, a fast decrease first occurs in time followed by a stabilization of the D1stN. Lastly, at 200 Pa, the D1stN value increases with time from the beginning of the

experiment. By comparing these results with the images obtained, it can be concluded that different aggregation mechanisms are governing the PGM particles behavior in the glass melt.

### *3.4 Aggregation mechanisms*

As shown in Figure 4, we can separate the conducted experiments in three different shear regimes: low shear (M1), medium shear (M2) and high shear (M3). They represent also the different aggregation mechanisms involved in the glass melt. The image analysis alone does not allow to differentiate the distinct kinetics that the material undergoes for the different imposed stresses. By associating the images with the D1stN, a detailed scenery is clarified. Figure 9 presents the average distance distribution of the particles first neighbor for all studied stresses, separated in three groups. The distance value is normalized by the initial distance (D1stNm) (at time  $t = 1200$  s for 0.1 Pa and 2 Pa, Figure 9a; and  $t = 300$  s for the other stress values, Figure 9b and c) versus the normalized time ( $t/t_m$ ).  $t_m$  is the final experimental time for each investigated situation. The distance points are illustrated by the associated images produced via the Python code described in section 3.2.

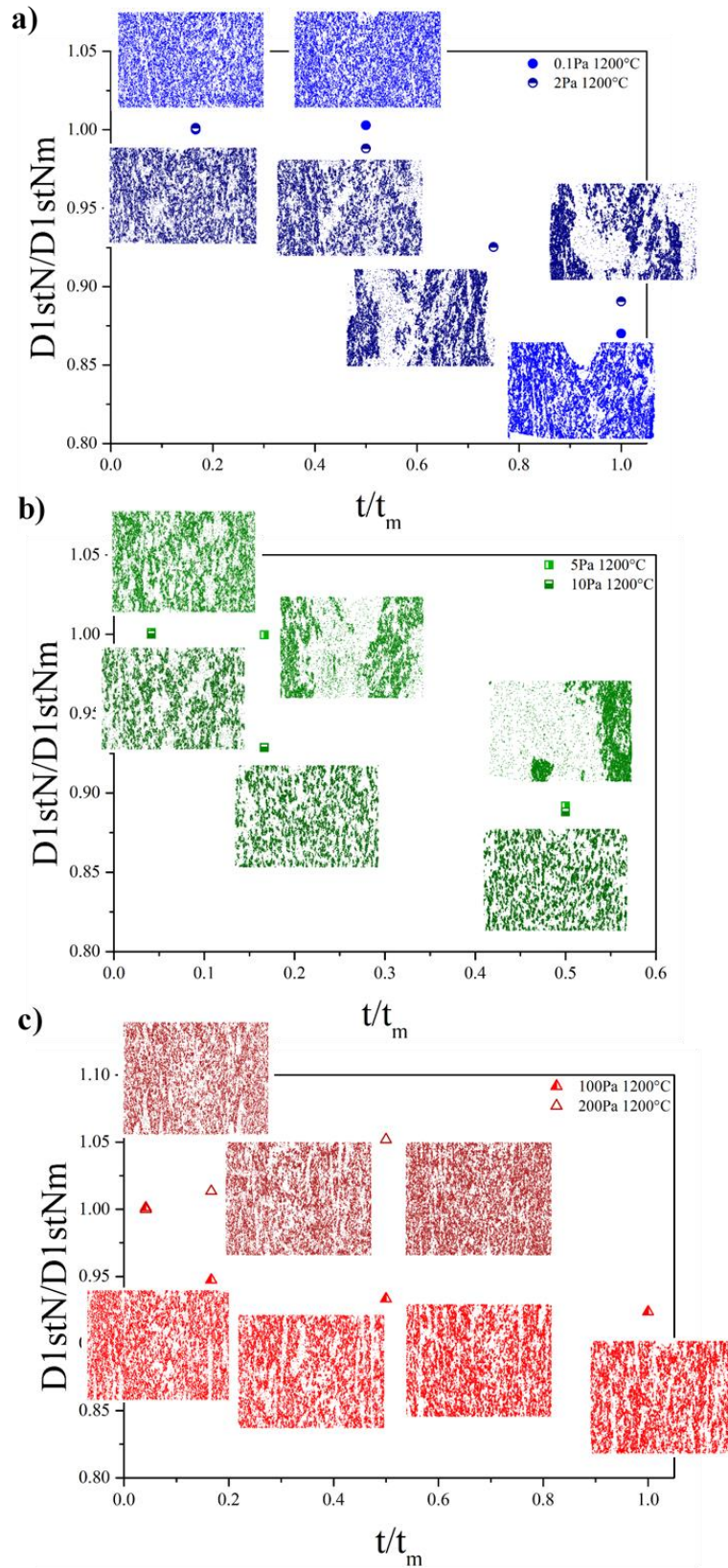


Figure 9 – Normalized D1stN as a function of the normalized time for all studied stresses, separated in three flow regimes, along with the Cartesian representation of the PGM structural units positioning: a) low shear stress (M1), b) medium shear stress (M2) and c) high shear stress (M3).

To interpret the behavior, we base this discussion on the so-called DVLO theory [14], [15]. This theory was developed to explain the aggregation of aqueous dispersions. In DLVO theory, aggregation of dispersed particles is explained by the interplay between attractive (including van der Waals, electrostatic attractive, hydrophobic, bridging, and depletion) and repulsive (including electrostatic double-layer force, steric, hydration, and structural) forces. Van der Waals forces, between identical particles, are always attractive and consequently promote aggregation, while double-layer force stabilize the dispersion keeping the particles apart. Their intensities do not depend on the external shear rate imposed by the rheometer. Thus, once aggregation is taking place in the investigated scenario, one can state that attractive forces predominate over repulsive ones. However, in the presently studied case, the shear stress imposed by the rheometer generates hydrodynamic forces, which influence the aggregation of the PGM particles. These forces, depending on their intensities, might favor or prevent particle aggregation as we are going to see.

For the low shear stress regime (M1), represented by Figure 9a, a decrease of the normalized  $D_{1stN}$  with time is noticed for both stresses. In this regime, the hydrodynamic forces imposed by the rheometer are weak and not enough strong to push the particles away from each others, so that van der Waals attraction dominates in this situation. Therefore, in this M1-scenario, particles can undergo aggregation and clusters are formed. Focusing on the images at  $t/t_m = 1$  under low shear stresses, the sample at 2 Pa exhibits a blatant heterogeneity. It indicates that for this shear stress range, the low hydrodynamic forces promote positive collisions and favor particle aggregation. In this first regime, the higher the stress, the quicker is the aggregation kinetics leading to a smaller distance between the clusters ( $D_{1stN}$ ). This particles rearrangement is correlated to the Newtonian plateau at low shear, which was observed in the steady state rheological tests (Figure 4). The particle-particle interactions that lead to the

aggregation have dramatic effects on viscosity since not only are the aggregates larger than the individual particles, and hence more resistant to flow, but they also enclose, and so immobilize some of the liquid phase, increasing their effective volume fraction, resulting in a higher viscosity at low shear rates [25].

Figure 9b shows the results for the medium shear stress regime (M2). This shear range is characterized by a decrease on viscosity when compared to the low shear regime M1, but with a steeper descent. Nonetheless, the same dynamic is observed as in the M1 regime: a decrease in  $D_{1stN}$  with time. Although the dependence is the same, the difference lays in the kinetics of the phenomenon. When the shear is increased above a critical stress, the hydrodynamic forces increase enough to counteract the aggregation phenomena, controlled by Brownian motion. The imposed shear stress is not high enough to disperse completely the particles but it enhances the local reorganizations. Differently from the first mechanism, when the stress is increased, the aggregates size reached after one hour decreases.

At a given shear stress or shear rate, the steady state is reached when a dynamical equilibrium is established between breakdown and reformation of the aggregates, leading to a mean equilibrium of the clusters radius. It will reach its maximum equilibrium size at the maximum imposed stress that it can support without breaking [26]–[28]. This radius will decrease as the shear increases, and consequently the viscosity will also decrease, which is associated to the shear-thinning behavior of suspensions. Even though the aggregates are smaller, the distance between particles keeps decreasing. This is due to a competition between cohesive forces caused by the fluid and rupture forces caused by the flow [29].

The results concerning the third studied regime (regime M3) are presented in Figure 9c. This regime is also characterized by a Newtonian plateau at high shear on the steady state rheograms.

Contrarily to mechanism M1 explained earlier, in which particles aggregation dominates, for high shear flow the hydrodynamics forces control the behavior of the suspension, causing the rupture of the aggregates. The distance between the SUs stabilizes over time at this range. As shown in Figure 9c, the PGM particles are completely dispersed in the glass matrix. This dispersion leads to greater first neighbor distances of the particles compared to the other regimes.

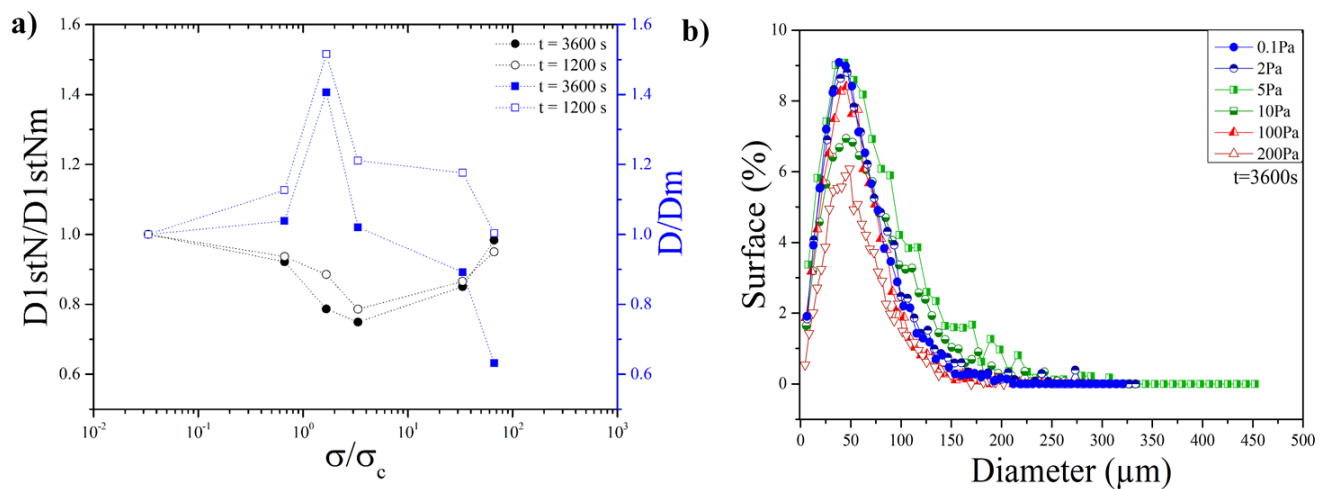


Figure 10 – a) Normalized D1stN and normalized F ret diameter (D) as a function of the normalized shear stress for experimental durations  $t = 3600$  s and  $t = 1200$  s. b) Surface percentage as a function of the cluster diameters for all the 3600s-samples studied.

In order to analyze the overall impact of the shear stress in the aggregation degree of the material, the three regimes were compared at two experimental durations for varying applied shear stress. Figure 10a shows the dependency of the normalized D1stN ( $D1stN/D1stNm$ ) versus the normalized shear stress ( $\sigma/\sigma_c$ ) at two different experimental times:  $t = 3600$  s and  $t = 1200$  s. The first neighbor distance is normalized by the initial value ( $D1stNm$ ) of sample  $\sigma = 0.1$  Pa. The critical shear stress is chosen at the end of the first Newtonian plateau,  $\sigma_c = 3$  Pa as shown in Figure 4. The distance to the first neighbor decreases with the stress for the low and medium shear flows. For both regimes M1 and M2, as previously mentioned, aggregation predominates, unlike for the high shear regime (M3), the first neighbor distance starts to

increase again. Figure 11 shows the corresponding Cartesian representations for each case presented in Figure 10a. It is noticed that the particles aggregation increases with the shear stress up to 10 Pa; above 10 Pa, further increase of the stress produces particles dispersion as shown in Figure 10a, even though images at 10, 100 and 200 Pa seem similar in Figure 11.

At this point, it is important to recall the definition of the structural units previously proposed. If we consider the SUs as small clusters composed of a few RuO<sub>2</sub> needles and Pd-Te spheres, the aggregates are clusters composed of SUs. Hence, the aggregates exhibit larger radii than the SUs. With the image analysis, it is possible to extract the size of the clusters present in the sample, or more precisely their maximum F eret diameter. In Figure 10b, the surface percentage occupied by the clusters as a function of their diameters is plotted for all the 3600 s samples. At first, it is noticed that all samples show a similar particle size distribution. This confirms the SU hypothesis since all samples would have a majority of small clusters of approximately 50  m dispersed in the matrix, which correspond to the average size of the SUs previously measured by SEM in the glass [4]. It is paradoxically found that the average distance to the first neighbor at low and high shear are similar, so the clusters diameter presented in Figure 10b helps explaining this paradox. For the medium and low shear stresses, contrary to the high shear stress regime, clusters of diameters greater than 300 and 450  m, that is to say aggregates, are observed. The same tendency appears when the normalized mean diameter of the clusters ( $D/D_m$ ) is plotted in Figure 10a as a function of the normalized shear stress for the 1200 and 3600 s experiments. After reaching a maximum size at 5 Pa, the diameter drops reaching a smaller cluster size than at 0.1 Pa. Therefore, when comparing the  $D_{1stN}$  for the low and high regimes, the values correspond to the  $D_{1stN}$  between aggregates and structural units, respectively. Even though the values are similar, for higher shear stresses, the structure is a collection of small clusters and individual particles.

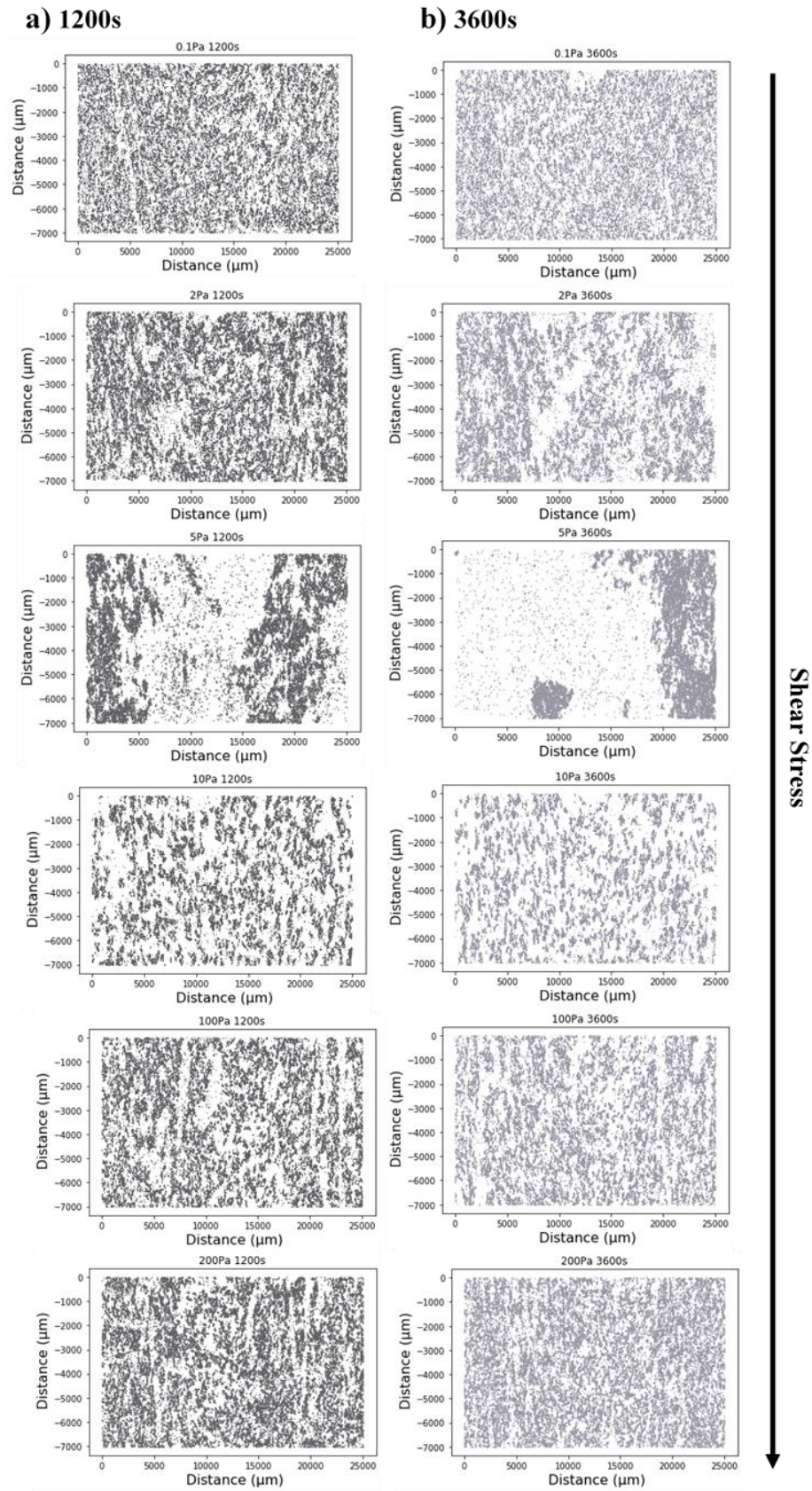


Figure 11 - Cartesian representations of the PGM structural units positioning in the top of the glass samples for all studied stresses at a) 1200 s and b) 3600 s.

### 3.5 Force balance and aggregation mechanisms

As mentioned earlier, the aggregation mechanisms experienced in this work can be explained based on DVLO theory [14], [15]. The three different mechanisms consist in a balance between the forces acting on the material, and for this work only two are considered: the hydrodynamic forces generated by the shear flow and the attractive van der Waals potential between the particles [30][31]. These two forces are estimated through the relations provided by Allain *et al.* [30]. The electrostatic forces are ignored in the present section, due to their difficult evaluation. The hydrodynamic force is calculated as  $F_H = \eta_f \dot{\gamma} R^2$ , where  $\eta_f$  is the viscosity of the continuous phase,  $\dot{\gamma}$  is the shear rate and  $R$  is the aggregate radius. For the van der Waals potential, the relation  $F_{vdW} = \frac{\Lambda a}{12h^2}$ , was considered, where  $\Lambda$  is the Hamaker constant,  $a$  is the particle radius and  $h$  is the mean distance between the particles.

Figure 12 shows the ratio between both forces as a function of  $\dot{\gamma}/\dot{\gamma}_c$ , where  $\dot{\gamma}_c = \sigma_c/\eta_0$  is the critical shear rate at which the viscosity abruptly decreases (the critical stress  $\sigma_c$  and the low shear viscosity  $\eta_0$  are indicated in Figure 4). The forces were approximated using the data obtained for the 3600 s experiments at all studied shear stresses. To adapt the equations to experimental reality, the viscosity of the continuous matrix was considered the viscosity of the technological molten glass without PGM particles ( $\eta_f = 3.6$  Pa.s) and the radius of the particles  $a$  as the mean size of the SUs ( $a = 50 \mu m$ ). The aggregate radius ( $R$ ) and the mean distance between the particles ( $h$ ) are the mean F eret radius of the SUs and the D1stN for the 3600 s experiments, respectively (showed in Figure 10a). Since there is a lack of information on Hamaker constant for silicate melts in the literature, a range of values was scanned.

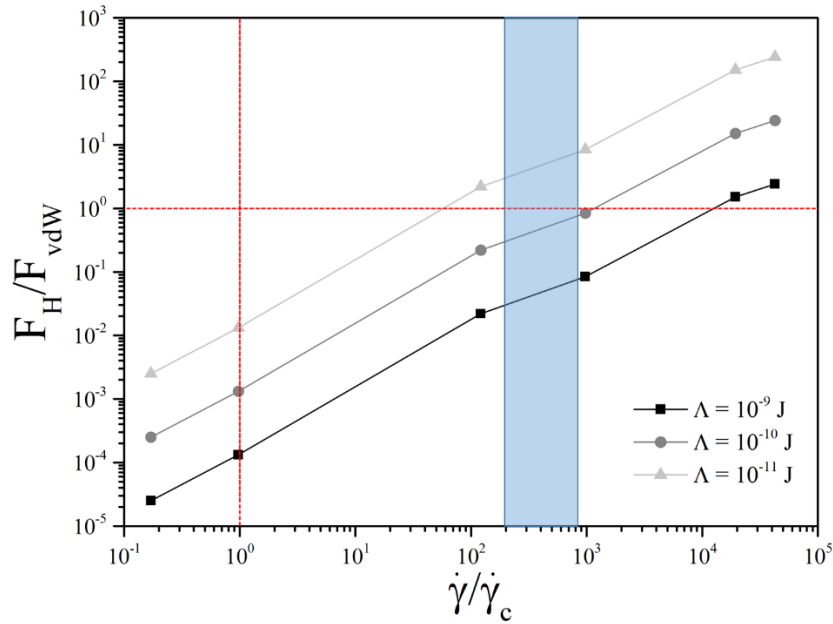


Figure 12 – The ratio between the hydrodynamic forces ( $F_H$ ) and the van der Waals potential ( $F_{vdW}$ ) as a function of  $\dot{\gamma}/\dot{\gamma}_c$ , for three different Hamaker constants.  $\dot{\gamma}_c$  is the critical shear rate when the viscosity abruptly decreases.

When analyzing the graph, it is noticed that below the critical shear rate ( $\dot{\gamma}/\dot{\gamma}_c \leq 1$ ), the van der Waals potential has a greater impact on the melt, as predicted for mechanism M1. For a shear above the critical value, the impact of the hydrodynamic force increases but the ratio  $F_H/F_{vdW}$  is still under one, indicating that van der Waals attraction is still affecting the particles reorganization in the melt. Hence the critical shear rate indicates only the limit between the two recognized rheological behaviors of the material (Newtonian and the shear thinning), not being directly connected to the moment where the hydrodynamic forces surpass the binding forces between particles. Considering a Hamaker constant between  $10^{-10}$  and  $10^{-11}$  J, the force balance corresponds to the hypothesis that the increase of the hydrodynamic forces and beginning of the mechanism M3 happens when the shear is more than a hundred times the critical shear, corresponding to the shaded region of the graph. In terms of shear stress, it corresponds to more than 10 Pa, which matches with the smaller clusters showed in Figure 11 that are formed after 3600 s due to the competition between the aggregation and dispersion of the SUs in the melt.

## 4 Conclusions

The aggregation mechanisms of a simulated nuclear glass melt containing 3 wt% of PGM particles was studied in this paper. The impact of the shear stress and time on the PGM particles aggregation degree was determined using a stress-imposed rheometer working at high temperature, and an SEM image analysis method. Given the impossibility of in situ analysis at 1200 °C, a post-mortem approach was chosen where each sample was submitted at 1200°C to different shear stresses and for different durations. The choice of durations aimed to capture the evolution of the particles rearrangement with the viscosity, from the early stages of the regime to the steady state. For a same stress applied for different durations, the samples showed the same rheological behavior as a function of time, validating the reproducibility of the employed protocol.

Image mosaics obtained for each sample were submitted to an image treatment aiming to highlight the structural units (SU) made of RuO<sub>2</sub> needles and Pd-Te spherical particles, and their distribution in the glass. This image analysis was an important tool to evidence the aggregation degree of each sample, highly influenced by the experiment time. Although visually the aggregation was clear, a numerical approach was developed translating the distance between the first near neighbor of the particles in a parameter to quantify the aggregation in each sample. The overall data showed that the PGM glass behaves in three different ways depending on the flow regime at which it is imposed *i.e.*, low, medium and high shear flow regime. An explanation of the three mechanisms is proposed in this work.

The three mechanisms differentiate themselves by the intensity of the forces acting in the particles. For the first regime, a combination of the low hydrodynamics forces and van der Waals attractive forces on the PGM particles contributes for the aggregation phenomenon,

translated by the decrease in the distance between clusters. It affects the viscosity by increasing the volume fraction leading to a higher viscosity at low shear rates. At a medium flow, the same forces are acting in the particles, but in a different ratio than the low shear regime: the hydrodynamic forces have also an impact, enhancing local reorganizations but are not strong enough to dissipate the particles in the glass. The viscosity decreases significantly, but the aggregation still occurs, which is showed by the continuous drop of distance values. At high shear flow, the particles are completely dispersed in the melt due to the effects of the hydrodynamic forces, leading to a higher distance between the particles and a low viscosity. The experimental challenges of observing the aggregation kinetics of PGM particles in a glass melt are overcome thanks to a numerical approach that allows to quantify the evolution of aggregation and its impact to construct the general idea of what influences the phenomena. A balance between the hydrodynamic forces and van der Waals potential was estimated using the collected data to support the work hypothesis. The information collected can be linked directly to the rheological behavior of the PGM glass, adding a deeper comprehension of the material and consequently to the vitrification process.

## **5 Acknowledgements**

The *Commissariat à l'Énergie Atomique et aux Énergies Alternatives* (CEA) and Orano are gratefully acknowledged for the financial support provided. The authors also would like to thank Sylvain Mure, Henri-Pierre Brau and Charlène Vallat for the valuable help in the experimental part of the work, and for the fruitful discussions on SEM and image treatment. Dr. Luiz Pereira thanks the *Ludwig-Maximilians-Universität München* for the provided ERC-GA-834225 post-doctoral grant.

## 6 References

- [1] E. Vernaz, S. Gin, and C. Veyer, “Waste glass,” *Compr. Nucl. Mater.*, vol. 5, no. January, pp. 451–483, 2012, doi: 10.1016/B978-0-08-056033-5.00107-5.
- [2] R. F. Taylor, “Chemical engineering problems of radioactive waste fixation by vitrification,” *Chem. Eng. Sci.*, vol. 40, no. 4, pp. 541–569, 1985, doi: 10.1016/0009-2509(85)80001-4.
- [3] T. Akai, J. Nishii, M. Yamashita, and H. Yamanaka, “Chemical behavior of platinum-group metals in oxide glasses,” *J. Non. Cryst. Solids*, vol. 222, pp. 304–309, 1997.
- [4] B. Luckscheiter and C. Krause, “Properties and behavior of the platinum group metals in the glass resulting from the vitrification of simulated nuclear fuel reprocessing waste,” *J. Mater. Res.*, vol. 6, no. 12, pp. 2535–2546, 1991, doi: 10.1557/JMR.1991.2535.
- [5] W. Grünewald, G. Roth, W. Tobie, K. Weiß, and S. Weisenburger, “The role of the platinum group elements ruthenium, rhodium and palladium in the vitrification of radioactive high level liquid waste using joule heated ceramic lined waste glass melters,” *Glas. Technol. Eur. J. Glas. Sci. Technol. Part A*, vol. 49, no. 6, pp. 266–278, 2008.
- [6] F. Pacaud, C. Fillet, and N. Jacquet-Francillon, “Effect of platinoids on French LWR reference glass properties,” *Mater. Res. Soc. Symp. Proc.*, vol. 257, no. 3, pp. 161–167, 1992.
- [7] S. Vargas, “Straw and Coal Ash Rheology,” Technical University of Denmark, 2001.
- [8] C. Hanotin, J. Puig, M. Neyret, and P. Marchal, “Platinum group metal particles aggregation in nuclear glass melts under the effect of temperature,” *J. Nucl. Mater.*, vol. 477, pp. 102–109, 2016, doi: 10.1016/j.jnucmat.2016.04.033.
- [9] K. Uruga, T. Usami, T. Tsukada, S. Komamine, and E. Ochi, “Viscoplasticity of

- simulated high-level radioactive waste glass containing platinum group metal particles,” *J. Nucl. Mater.*, vol. 452, no. 1–3, pp. 419–424, 2014, doi: 10.1016/j.jnucmat.2014.05.062.
- [10] J. Puig, B. Penelon, P. Marchal, and M. Neyret, “Rheological Properties of Nuclear Glass Melt Containing Platinum Group Metals,” *Procedia Mater. Sci.*, vol. 7, pp. 156–162, 2014, doi: 10.1016/j.mspro.2014.10.021.
- [11] J. Puig, C. Hanotin, M. Neyret, and P. Marchal, “High temperature rheological study of borosilicate glasses containing platinum group metal particles by means of a mixer-type rheometer,” *J. Nucl. Mater.*, vol. 469, pp. 112–119, 2016, doi: 10.1016/j.jnucmat.2015.11.053.
- [12] Y. Yue and R. Brückner, “A new description and interpretation of the flow behaviour of glass forming melts,” *J. Non. Cryst. Solids*, vol. 180, no. 1, pp. 66–79, 1994, doi: 10.1016/0022-3093(94)90398-0.
- [13] F. Babick, *Suspensions of Colloidal Particles and Aggregates*, vol. 20. 2016.
- [14] C. E. Marshall, “‘Theory of the stability of lyophobic colloids. The interaction of particles having an electric double layer.’ E. J. W. Verwey and J. T. G. Overbeek, with the collaboration of K. van Ness. Elsevier, New York-Amsterdam, 1948, 216 pp.,” *J. Polym. Sci.*, vol. 4, no. 3, pp. 413–414, Jun. 1949, doi: 10.1002/pol.1949.120040321.
- [15] B. Derjaguin and L. Landau, “Theory of the stability of strongly charged lyophobic sols and of the adhesion of strongly charged particles in solutions of electrolytes,” *Prog. Surf. Sci.*, vol. 43, no. 1–4, pp. 30–59, 1993, doi: 10.1016/0079-6816(93)90013-L.
- [16] C. Bower, C. Washington, and T. S. Purewal, “The use of image analysis to characterize aggregates in a shear field,” *Colloids Surfaces A Physicochem. Eng. Asp.*, vol. 127, no. 1–3, pp. 105–112, 1997, doi: 10.1016/S0927-7757(96)03945-3.
- [17] A. Kurokawa, V. Vidal, K. Kurita, T. Divoux, and S. Manneville, “Avalanche-like

- fluidization of a non-Brownian particle gel,” *Soft Matter*, vol. 11, no. 46, pp. 9026–9037, 2015, doi: 10.1039/c5sm01259g.
- [18] S. Deboeuf, N. Lenoir, D. Hautemayou, M. Bornert, F. Blanc, and G. Ovarlez, “Imaging non-Brownian particle suspensions with X-ray tomography: Application to the microstructure of Newtonian and viscoplastic suspensions,” *J. Rheol. (N. Y. N. Y.)*, vol. 62, no. 2, pp. 643–663, 2018, doi: 10.1122/1.4994081.
- [19] T. Advocat, J. L. Dussossoy, and V. Petitjean, “Vitrification des déchets radioactifs et appareillage,” *Les Tech. l’Ingénieur*, vol. 33, no. 0, pp. 0–27, 2008.
- [20] M. Bousmina, A.-S. Chrissemant, L. Choplin, A. Aït-Kadi, and P. Marchal, “Quantitative Analysis of Mixer-Type Rheometers using the Couette Analogy,” *Can. J. Chem. Eng.*, vol. 80, no. December, pp. 1166–1174, 2010, doi: 10.1002/cjce.5450800618.
- [21] Bousmina M.; A. Aït-Kadi and J.B. Faisant, “Determination of Shear Rate and Viscosity from Batch Mixer Data: Theoretical and Experimental Results,” *J. Rheol.*, vol. 43, p. 1999, 1999.
- [22] W. L. Wang, J. Q. Bi, K. N. Sun, M. Du, N. N. Long, and Y. J. Bai, “Thermal shock resistance behavior of alumina ceramics incorporated with boron nitride nanotubes,” *J. Am. Ceram. Soc.*, vol. 94, no. 8, pp. 2304–2307, 2011, doi: 10.1111/j.1551-2916.2011.04658.x.
- [23] O. Delattre, E. Régnier, S. Schuller, M. Allix, and G. Matzen, “Image analysis study of crystallization in two glass compositions of nuclear interest,” *J. Non. Cryst. Solids*, vol. 379, pp. 112–122, 2013, doi: 10.1016/j.jnoncrysol.2013.07.029.
- [24] J. Fournier-Renaud, “Cinétiques de dissolution des cristaux dans les silicates fondus – contexte des verres nucléaires,” Université Montpellier, 2017.
- [25] W. R. Richmond, R. L. Jones, and P. D. Fawell, “The relationship between particle

- aggregation and rheology in mixed silica-titania suspensions,” *Chem. Eng. J.*, vol. 71, no. 1, pp. 67–75, 1998, doi: 10.1016/S1385-8947(98)00105-3.
- [26] H. A. Barnes, *A Handbook of Elementary Rheology*. The University of Wales- Institute of Non-Newtonian Fluid Mechanics, Department of Mathematics, 2000.
- [27] D. B. Genovese, “Shear rheology of hard-sphere, dispersed, and aggregated suspensions, and filler-matrix composites,” *Adv. Colloid Interface Sci.*, vol. 171–172, pp. 1–16, 2012, doi: 10.1016/j.cis.2011.12.005.
- [28] P. Snabre and P. Mills, “Rheology of concentrated suspensions of viscoelastic particles,” *Colloids Surfaces A Physicochem. Eng. Asp.*, vol. 152, no. 1–2, pp. 79–88, 1999, doi: 10.1016/S0927-7757(98)00619-0.
- [29] V. A. Tolpekin, M. H. G. Duits, D. Van Den Ende, and J. Mellema, “Aggregation and breakup of colloidal particle aggregates in shear flow, studied with video microscopy,” *Langmuir*, vol. 20, no. 7, pp. 2614–2627, 2004, doi: 10.1021/la035758l.
- [30] C. Allain, M. Cloitre, and F. Parisse, “Settling by cluster deposition in aggregating colloidal suspensions,” *J. Colloid Interface Sci.*, vol. 178, no. 2, pp. 411–416, 1996, doi: 10.1006/jcis.1996.0135.
- [31] F. E. Torres, W. B. Russel, and W. R. Schowalter, “Floc structure and growth kinetics for rapid shear coagulation of polystyrene colloids,” *J. Colloid Interface Sci.*, vol. 142, no. 2, pp. 554–574, 1991, doi: 10.1016/0021-9797(91)90086-N.